*https://doi.org/10.46813/2022-137-026*

UDC 537.311.33.539.1.074.669.054

# STRUCTURAL FEATURES OF DOPED SILICON SINGLE CRYSTALS

***N.A. Azarenkov, V.E. Semenenko, N.G. Stervoyedov***
***V.N. Karazin Kharkiv National University, Kharkiv, Ukraine***
***E-mail: azarenkov@karazin.ua***

The nature of the change in the Fermi level of silicon under the influence of dopants, point defects, and dislocations has been determined. The parameters of the diffusion of impurities, the conditions for their appearance and removal in the process of directional crystallization and the post-crystallization period have been established. The expediency of doping silicon with boron and phosphorus was shown, and large single crystals were obtained. The mechanisms of elimination of structural defects have been clarified. The mobility and lifetime of charge carriers in perfect silicon single crystals under radiation exposure have been determined. The expediency of using *p*-type silicon as a base material for solar modules for space purposes is shown.

## INTRODUCTION

Energy supply is one of the basic factors of the country's security and well-being. A promising basis for alternative energy is the direct conversion of solar radiation energy into electrical energy using semiconductor materials [1, 2].

At a distance of 150 million km from the Sun, whose luminosity is $3.8 \cdot 10^{23}$ kW, the Earth receives ~ $10^{17}$ W of solar energy. Average annual solar radiation falling on the territory of Ukraine is 1000…1600 (kW·h)/m$^2$. With the help of heliostats or mirrors, you can increase the flow of solar energy to the surface of solar transducers). In low-temperature solar installations (SPP), solar radiation of natural density (0.8 kW/m$^2$) is used, in high-temperature – the density is increased by $10^2$…$10^4$ times, using solar concentrators. The average capacity of solar power plants (SPP) is 0.1…10 MW, reaching 100 MW.

The distribution of alternative energy production by different countries is shown in Fig. 1. In the next decade, the share of alternative energy in the EU countries will increase to 40%. The predominant basis of materials for solar energy is the most available silicon in nature. Doped silicon with amorphous, film, poly- and monocrystalline structures is used in semiconductor technology.

When studying thin films of semiconductor materials, manifestations of size effects (classical and quantum) are possible, which have a significant effect on the kinetic and thermoelectric properties of semiconductor materials [3]. A high value of the carrier mobility was found in $A^{III}B^{V}$ semiconductor compounds (GaSb, AlSb, AsGa, ...). $A^{II}B^{VI}$ (CdTe) semiconductors are used as radiation detectors. In optoelectronics, $A^{II}B^{VI}$ (PbSe) compounds are used, quantum heterostructures are obtained in InAs/GaP [3, 4].

The quality level of high-resistance silicon largely determines the quality of devices and devices of solid-state electronics, solar module elements, etc. manufactured on its basis [5].

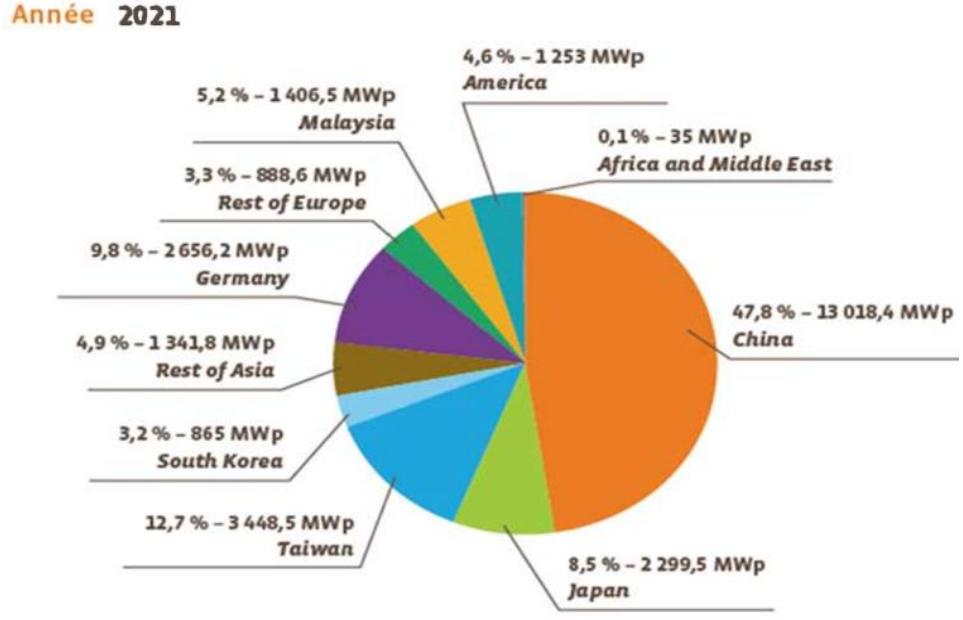


*Fig. 1. Distribution of alternative energy generation by different countries*

## EXPERIMENTAL RESULTS AND DISCUSSION

Silicon is an indirect-gap semiconductor that absorbs in the frequency range of light with a quantum energy slightly greater than the band gap $E_g = (1.21 \dots 3.6) \cdot 10^{-4} T$, optimal $E_g \approx 1.3 \dots 1.4$ eV) only due to indirect transitions, the intensity of which depends on the presence of phonons and, consequently, on temperature.

The cutoff frequency of indirect silicon transitions is > 3 eV, that is, it lies in the ultraviolet region of light [2].

Literary sources indicate the degradation of the properties of solar cells (SC), which is determined by the method of their manufacture, structural-phase state, coefficient of light reflection from the surface of solar cell plates and the type of dopants affecting the mobility of current carriers [6, 7]. For the successful production of solar modules – a material for space and special purposes, detailed macro- and microstructural, phase studies are required. However, similar data are very limited. This work is devoted to the study of the above problems.

In the present work, silicon single crystals doped with acceptor and other impurities with a perfect structure were obtained using the method of controlled phase transformation (directional crystallization), which makes it possible to control the macro- and microstructure, morphology of structural components [2, 6].

The high purity of the initial matrix materials (silicon) used to create SC is due to the low concentration of dopants ($10^{-5} \dots 10^{-7}$ wt.%), sufficient to change the electrophysical properties of semiconductors. The specific resistance $\rho$ of pure silicon is $\rho_{Si}$~$10^3$ Ω·cm. The specific resistance of doped silicon $\rho_{Si} + 10^{-3}$ at.% P is 0.006 Ω·cm.

The energy losses of impurities in silicon have been studied (Fig. 2). The electron energy distribution is described by the Fermi-Dirac function:

$$f(E) = \frac{1}{e^{\frac{E-E_F}{KT}}+1}, \quad (1)$$

where $E_F$ is the Fermi energy.

In a pure semiconductor with an equal concentration of current carriers – free electrons and holes:

$$e^{-\frac{E_2-E_F}{KT}} = e^{-\frac{E_F-E_1}{KT}}. \quad (2)$$

Thus, $E_F = \frac{E_1+E_2}{2}$, the Fermi level lies in the middle of the band gap, the concentration of electrons and holes is $n \sim p \sim e^{-E_g/KT}$.

In a semiconductor doped with a donor impurity, the "tail" of the Fermi function (*f*) extends into the conduction band, greater than the "tail" of the Fermi function (*1-f*), extending into the valence band. That is, in such a semiconductor, the Fermi level is located closer to the conduction band. In contrast, in an acceptor semiconductor, the Fermi level is located closer to the valence band.

According to the literature, acceptor impurities of subgroup IIIA (B, Al, Ga, ...) and subgroup VA (P, As, Sb, ...) have a smaller cross-section for capture of current carriers than impurities of heavy and noble metals (Fe, Ni, W, ..., Cu, Ag, Au), which are used to obtain wide-gap semiconductors (GaAs, InP, ...) doped with Cr, Fe, Al [8].

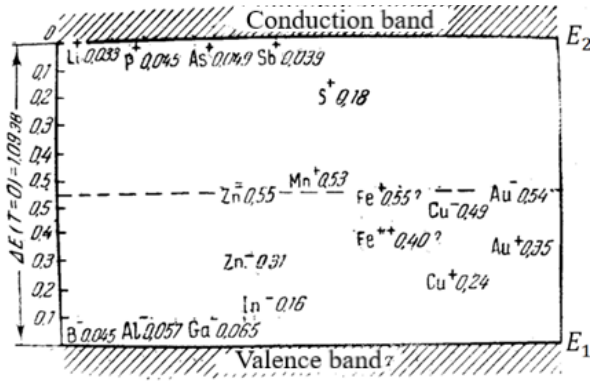


*Fig. 2. Energy losses of impurities in silicon*

As is known, the number of charge carriers changes depending on the type of impurity and their concentration. As can be seen from Fig. 2, impurities P and B create single energy levels in silicon crystals – donor, located in the upper half of the band gap, and acceptor, in the lower half of the band gap. This arrangement of the levels creates favorable conditions for their relatively easy ionization. Therefore, in a wide temperature range, impurities P and B are the main sources of carriers that change the conductivity of silicon.

The nature of the redistribution of impurities in the process of directional crystallization of silicon has been studied. The effective segregation coefficient of impurities is determined [2, 14]:

$$K_{эф} = \frac{K_0}{K_0 + [1 - K_0 \cdot e^{-\frac{R}{R_g}}]}, \quad (3)$$

where $R$ is the speed of movement of the solid-liquid interface, $R_g$ is the characteristic growth rate constant, which depends on the mixing of the melt and the diffusion coefficient of impurities in the melt, $R_g = \frac{Д}{\Delta}$, where Δ is the length of the diffusion layer at the interface.

It was determined that at R < 100 mm/h, equation (3) takes the following form:

$$K_{ef} = K_0 e^{-\frac{R}{R_g}}, \quad (4)$$

where $K_0$ is the equilibrium impurity distribution coefficient.

The distribution of impurities $N$ in the ingot obtained by slow radial cooling of the sample is determined as follows:

$$N = K_{ef} \cdot N_0 (1 - l)^{K_0 - 1}, \quad (5)$$

where $N$ is the concentration of impurities in the solid solution, $l$ is the relative fraction of the length of the crystallized part, which is counted from the beginning of the solidification boundary of the ingot, $N_0$ is the initial concentration of impurities in the melt.

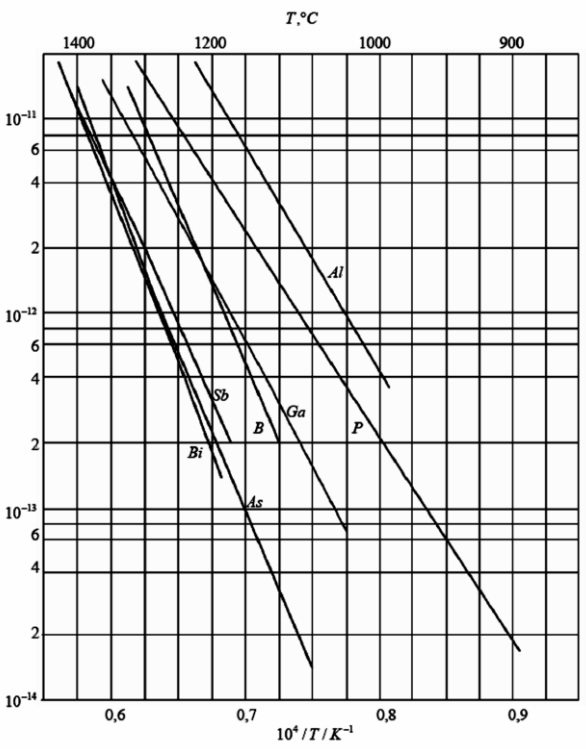


*Fig. 3. Temperature dependence of the diffusion coefficients of impurities in silicon*

According to Fig. 3, it is possible to estimate the maximum solubility of impurities in silicon at T > 1400…1600 K. It should be noted that impurities of Cu, Au, Li, ... diffuse along the interstices of the crystal lattice. The vacancy mechanism is characteristic of acceptor and donor impurities [2, 15, 16].

Table 1 shows the values of the effective distribution coefficients of impurities.

Table 1

Impurity distribution coefficients

| | | | | | | | |
|---|---|---|---|---|---|---|---|
| Li | $10^{-2}$ | P | 0.35 | Ni | $1\cdot10^{-4}$ | Zr | $2\cdot10^{-8}$ |
| B | 0.8 | S | $1\cdot10^{-5}$ | Cu | $1\cdot10^{-4}$ | Nb | $5\cdot10^{-7}$ |
| C | $7\cdot10^{-6}$ | Ti | $5\cdot10^{-6}$ | Zn | $1\cdot10^{-5}$ | Ta | $2\cdot10^{-8}$ |
| N | $7\cdot10^{-6}$ | V | $5\cdot10^{-6}$ | Ga | $8\cdot10^{-3}$ | Ag | $1\cdot10^{-4}$ |
| O | 1.25 | Cr | $5\cdot10^{-6}$ | Ge | 0.3 | Cd | $1\cdot10^{-6}$ |
| Na | $2\cdot10^{-3}$ | Mn | $1\cdot10^{-5}$ | As | 0.3 | Sb | $2\cdot10^{-2}$ |
| Mg | $2\cdot10^{-3}$ | Fe | $1\cdot10^{-5}$ | Mo | $5\cdot10^{-8}$ | Sn | $2\cdot10^{-2}$ |
| Al | $2\cdot10^{-3}$ | Co | $1\cdot10^{-5}$ | W | $5\cdot10^{-8}$ | Bi | $7\cdot10^{-4}$ |

According to the studies carried out, the most effective purification in the process of directional crystallization is observed for Zr, Mo, W, Ta, Nb, Cd, Bi, it is quite effective for Ti, V, Cr, Mn, Fe, Co, Zn, Ni, Cu, Ga, Ag, weaker – $O_2$, C, $N_2$.

It was found that the diffusion mobility of impurities is determined by the concentration of acceptor vacancies. Their acceptor level is located at a distance of 0.15 eV from the bottom of the conduction band [9].

As a result of changes (Fig. 4) in the design and composition of the growth unit assemblies (vacuum $P < 10^{-6}$ Torr, hydrogen or helium atmosphere), the use of tungsten heaters and boron nitride crucibles, the content of difficult-to-remove impurities was: $O_2$ – $2\cdot10^{15}…2\cdot10^{16}$, C – $2\cdot10^{16}…2\cdot10^{17}$, $N_2 < 1\cdot10^{12}$ $cm^{-3}$.

*Fig. 4. Crucible and elements of the heating unit of the growth unit*

The impurity composition of silicon alloys used to obtain single crystals is as follows: Si – 99.999, B – $1.3\cdot10^{16}cm^{-3}$, P – $6.8\cdot10^{16}cm^{-3}$. Methods for determining the composition of impurities and structural-phase composition are given in [2, 10].

In order to increase the spectral susceptibility of the surface of thin plates of SC, which were obtained by cutting massive crystals, a technique for anodic etching of *n*- and *p*-type silicon crystals was developed. It has been determined that the participation of charge carriers of different signs in the electrochemical reactions of a semiconductor determines the different behavior of *n*- and *p*-type single crystals.

On *p*-type silicon electrodes, in which holes are the main current carriers, the anodic process is unimpeded and the anodic behavior of the electrode is almost the same as for metal. In *n*-type silicon, holes are not the main current carriers and their concentration in the bulk of the semiconductor is small. As a result, the rate of the anodic process is determined by the rate of entry of holes to the electrode surface, which are formed as a result of generation in the space charge layer (Table 2).

Table 2

Etching modes

| Samples | Current density, $mA/cm^2$ | T, °C | Etching time $\tau$, min |
|---|---|---|---|
| *n*-type | 15…20 | 5…15 | 5…7 |
| *p*-type | 50…60 | 5…10 | 10…20 |

*Fig. 5. Crystallization of silicon alloys*

In the process of directional crystallization from the seed, spiral growth of the crystal was observed, which is consistent with the features of the outer surface of the ingot and explains the distribution of impurities in the

bulk of the crystal [2, 11]. Controlled parameters of structure formation, such as the temperature gradient at the interface *R* and the concentration of impurities *G*, determine the shape of the crystallization front and the size of the supercooled region. To prevent the inhomogeneous redistribution of impurities in the growing crystal, a magnetic field was applied (Fig. 5).

It was found that the concentration of acceptor and donor impurities, one atom per million, is sufficient to cover the grain boundaries of pure silicon with a layer of impurity atoms (Fig. 6). To eliminate large recombination losses, the grain size of a silicon SC must be several millimeters, which is important in the technology of creating solar modules.

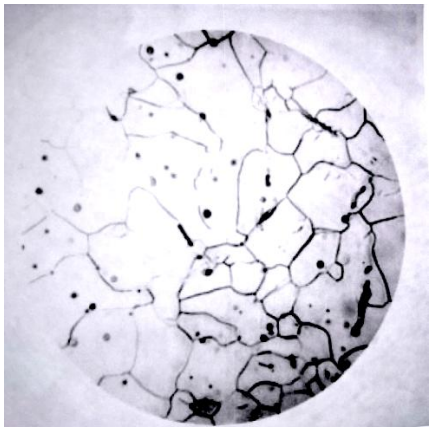

*Fig. 6. Microstructure of silicon alloys (x400)*

In the initial stage of crystallization, growth dislocations were found (Fig. 7). The single crystal topogram was determined by the Berg-Barrett method (Fig. 8). The topogram of a silicon single crystal was obtained when shooting in transmission under conditions of extinction contrast, in which defects (dislocations) are revealed as microvolumes with increased reflectivity. Loops of individual dislocations are clearly visible, evenly distributed over the volume. Accumulation of dislocations in the center are lined up in a dislocation grid. Fragments of the crystal substructure form boundaries with small angles.

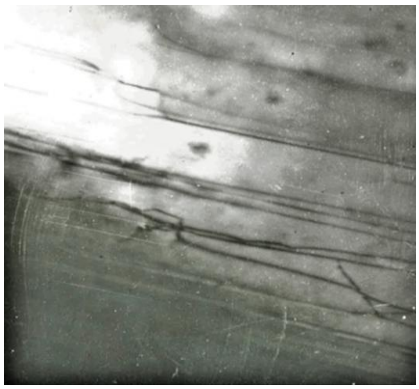

*Fig. 7. Growth dislocations (x30000)*

It was found that in the growing crystal there is a supersaturation with vacancies, amounting to $10^{17}…10^{18}$ $cm^{-3}$ at premelting temperatures and $10^{17}$ $cm^{-3}$ at 300 K. It was found that the supersaturation with vacancies is eliminated by the formation of clusters in the form of disks capable of flattening, forming dislocation loops in silicon crystals (Fig. 9)

Loop formation energy ~ 4.0 eV. The loop regions can represent stacking faults limited by partial dislocations [16].

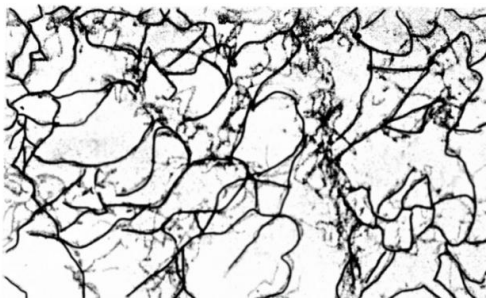

*Fig. 8. X-ray topogram of a silicon single crystal (x50)*

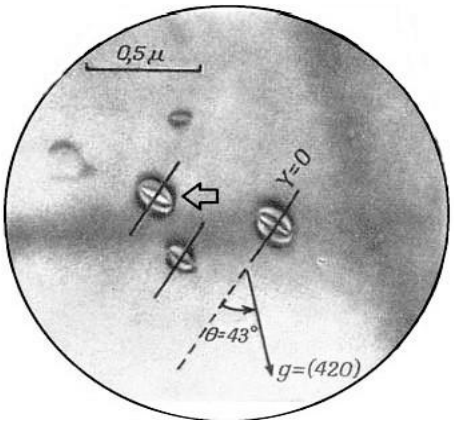


*Fig. 9. Dislocation loops in silicon crystal*

The conditions for the escape of dislocations from the growing crystal are investigated. It was found that due to the presence of anisotropy in the energy of the dislocation line, the propagation of dislocations in certain directions is minimized. According to Fig. 10, as the crystal grows, there is a gradual increase in the degree of perfection. The long, gently curving lines are likely formed by plastic flow at temperatures several hundred degrees below the melting point. Zigzag lines are made up of segments, which alternately are edge or screw dislocations. This indicates crawling and sliding in the region of the growing interface between the liquid and solid phases.

*Fig. 10. Edge and screw dislocations (x25000)*

It was found that with an increase in the angle between the density of the least slip and the direction of growth, a dislocation emerges onto the crystal surface without crossing the interface. In single crystals, the [100] and [111] growth directions are energetically more favorable than [110] and [211]. Single crystals with orientations [100] and [111] have a dislocation density $\rho_d \approx 10^2\,\text{cm}^{-2}$. Single crystals with orientations [110] and [211] have a dislocation density $\rho_d \approx 10^2\,\text{cm}^{-2}$. A different character of motion of edge and screw dislocations was found. It is energetically more favorable for the regions of edge dislocations parallel to the Burgers vector [111] to move in the slip plane and dissociate. The complex structure of the screw dislocation, which is the source of hexagons, makes it difficult for them to leave the growing crystal. Thus, the screw dislocation remains "bound", and it is more difficult to "break" bonds in the bulk of the crystal. Therefore, in the most perfect silicon crystals ($\rho_d \approx 10^2\,\text{cm}^{-2}$), the "remaining" dislocations are screw dislocations.

It should be noted that after the creation of a perfect structure of single crystals, the subsequent change in the growth conditions (growth of the crystal to a large size) does not change the perfection of the structure, and allows the use of large crystals for the production of film solar cells.

The calculation of the mobility of nonequilibrium charge carriers in doped silicon crystals is carried out using an analytical approximation model that allows a good description of the experimental data in a wide temperature range $300\ \text{K} < T < 1400\ \text{K}$ and doping levels $10^{13}\text{cm}^{-3} \le N \le 10^{20}\text{cm}^{-3}$ in various direct-gap and indirect-gap semiconductors [12]. The data for calculating the charge mobility in silicon are given in Table 3.

The mobility of charge carriers is defined as follows:

$$\mu_i(N,T) = \mu_{max,i}(T_0)\frac{B_i(N)(\frac{T}{T_0})^{\beta_i}}{1+B_i(N)(\frac{T}{T_0})^{\alpha_i+\beta_i}}, \qquad (6)$$

where $B_i(N) = \left[\frac{\mu_{min,I}+\mu_{max,i}\left(\frac{N_{g,i}}{N}\right)^{\gamma_i}}{\mu_{min,I}-\mu_{max,i}}\right] \Big| T = T_0;$

$T_0 = 300$ K; $i = n, p$ for electrons and holes respectively; $N$ is the concentration of the dopant; $T$ is the temperature of the sample, the parameters $\mu_{min,I}$, $\mu_{max,i}, \alpha_i, \beta_i, \gamma_i$ depend on the type of semiconductor material; $\mu_{max,i}$ – mobility in lightly doped samples ($10^{-8}$ wt.%); $\mu_{min,I}$ – mobility under heavy doping conditions (~ 0.1 wt.% B, ~ 1 wt.% P); $N_g$ – concentration of charge carriers in an intrinsic semiconductor.

Table 3

Charge carrier parameters

| Charge carrier type | $\mu_{max}$, $\mu_{min}$, $\text{cm}^2/(\text{V}\cdot\text{s})$ | | $N_g$, $\text{cm}^{-3}$ | γ | α | β |
|---|---|---|---|---|---|---|
| Electrons | 1414.0 | 68.5 | $9.2\cdot 10^{16}$ | 0.71 | 2.42 | 0.26 |
| Holes | 470.5 | 44.5 | $2.2\cdot 10^{17}$ | 0.72 | 2.20 | 0.36 |

The results of calculated and experimental data based on measurements of the Hall effect and electrical conductivity show that the mobility of electrons is 3…3.5 times higher than the mobility of holes in the range of carrier concentrations in $10^{14}$ ... $10^{19}\text{cm}^{-3}$, at temperatures T = 800…1500 K.

It is known that the action of cosmic radiation leads to a decrease in the short-circuit current associated with a decrease in the lifetime and diffusion length of carriers [13]. The latter is due to the appearance of recombination centers in photoconverters. It was found that doping silicon with boron and phosphorus increases the lifetime of current carriers from several microseconds in undoped silicon to 9…10 s in doped silicon.

It was determined that the diffusion length of electrons generated by light in *p*-type silicon is greater than in *n*-type crystals. Hole silicon is found to be more radiation resistant than *n*-type silicon. Therefore, in silicon photoconverters for space purposes, the base ≤ material must have hole conductivity.

## CONCLUSIONS

The nature of the change in the Fermi level of silicon under the influence of impurity elements is determined. It is shown that the elements of groups III and V, forming interstitial and substitutional solid solutions, create electrically active centers, the local levels of which are located closer to the boundaries of the energy bands of the crystal. This arrangement of the levels creates favorable conditions for their relatively easy ionization.

The efficiency of doping silicon crystals with boron and phosphorus as the main sources of carriers that change the conductivity of silicon has been established. The diffusion mechanism in doped single crystals is determined, due to the difference in ionic radiuses and valences of boron, phosphorus and silicon.

It is shown that a decrease in all types of energy losses in photovoltaic converters with a directed improvement in the properties of a semiconductor material occurs as a result of the creation of a perfect optimal structure and a change in the band gap.

Large *p*- and *n*-type silicon single crystals have been grown by the method of controlled phase transformations. It is possible to manufacture from them defect-free SC for solar modules.

It is found that due to the anisotropy of the dislocation line with an increase in the angle between the density of the least slip and the direction of growth, dislocations emerge onto the crystal surface without crossing the interface. More perfect single crystals ($\rho_d \approx 10^2\,\text{cm}^{-2}$) obtained in the directions [100] and [111].

It has been determined that under conditions of radiation exposure, the lifetime of charge carriers in silicon crystals doped with phosphorus and boron is 9…10 s, which is much higher than that of undoped crystals. An increase in the mobility of 2.5…3 times in *p*-type crystals, with a carrier concentration of $10^{15}$ ... $10^{18}\,\text{cm}^{-3}$ shows the expediency of using *p*-type crystals as a material for silicon solar modules for space purposes.

## REFERENCES

1. А. Фаренбук, В. Бьюб. *Солнечные элементы: теория и эксперимент.* М.: «Энергоатомиздат», 2017, с. 149-154.
2. Н.А. Азаренков, В.Е. Семененко, В.И. Ткаченко. *Перспективные конструкционные материалы нетрадиционной энергетики*. Харьков: «ХНУ», 2016, с. 105.
3. E.I. Rogacheva, K.V. Novak. Effect of aging on the thermoelectric properties of the Bi2Te3 polycrystals and thin films // *Functional Materials*, 2021, N 19, p. 194-201.
4. O. Abramkin. Formation of InAs/GaP quantum heterostructures on silicon substrukt // *Functional materials.* 2021, N 19, p. 194-201.
5. Г.В. Гременюк, М.С. Тиванов, В.Б. Залесский. *Солнечные элементы на основе полупроводниковых материалов.* Минск: «МГУ», 2019, с. 35-124.
6. V.N. Shlegel. Yu. Borovlev, et al. Recent progress in oxide scintillation crystals development by low-thermal gradient Czochralski technique for particle physics experiments // *JINST*, 2017, v. 2, p. 272.
7. Aparna Das. *Recent development in semipollar InGaN lazer diods*. 2021, v. 19, p. 272-282.
8. E. Rogacheva et al. Semiconduction materials // *J. Electronic Materials.* 2010, p. 115.
9. Х. Меррер. *Диффузия в твердых телах*. Долгопрудный: «Интеллект», 2011, с. 404-480.
10. Н.А. Азаренков, В.Е. Семененко, С.В. Литовченко. *Фазовые превращения и диаграммы состояния*. Харьков: «ХНУ», 2006, 101 с.
11. Ю.И. Таран, А.С. Регель и др. Структурные превращения при нагреве монокристаллов кремния // *ФТП.* 2016, №35, в. 4, с. 533-545.
12. Т. Мнацаканов, М.Е. Левинштейн. Универсальный метод аналитической аппроксимации подвижности основных носителей заряда в полупроводниках в широком диапазоне температур и уровней легирования // *ФТП*, 2004, т. 38, в. 1, с. 56-60.
13. Л.С. Новиков. *Радиационное воздействие на материалы космических аппаратов*. М.: «МИФИ», 2019, с. 78-91.
14. Н.А. Азаренков, В.Е. Семененко, Н.Г. Стервоедов. Влияние диффузионных процессов на структурную стабильность естественных микрокомпозитов // *Вопросы атомной науки и техники.* 2011, №2(97), с. 149-154.
15. R.M. Peleshak, O.V. Kuzyk, Formation of periodic structure under influence of an acoustic wave in semiconductor // *Ukr. J. Phys.* 2016, v. 61, N 1, p. 28-40.
16. I.V. Horichok, H. Hurhula. Semiempirical energies ofvacancy formation in semiconductor // *Ukr. J. Phys.* 2016, v. 61, N 1, p. 27-38.


*Article received 28.10.2021*

## СТРУКТУРНЫЕ ОСОБЕННОСТИ ЛЕГИРОВАННЫХ МОНОКРИСТАЛЛОВ КРЕМНИЯ

***Н.А. Азаренков, В.Е. Семененко, Н.Г. Стервоедов***

Определен характер изменения уровней Ферми кремния под влиянием легирующих примесей, точечных дефектов и дислокаций. Установлены параметры диффузии примесей, условия их возникновения и удаления в процессе направленной кристаллизации и в посткристаллизационный период. Показана целесообразность легирования кремния бором и фосфором, получены крупные монокристаллы. Выяснены механизмы ликвидации структурных дефектов. Определена подвижность и время жизни носителей заряда в совершенных монокристаллах кремния в условиях радиационного воздействия. Показана целесообразность применения кремния *p*-типа в качестве материала базы солнечных модулей космического назначения.

## СТРУКТУРНІ ОСОБЛИВОСТІ ЛЕГОВАНИХ МОНОКРИСТАЛІВ КРЕМНІЮ

***М.О. Азарєнков, В.Є. Семененко, М.Г. Стервоєдов***

Визначено характер зміни рівня Фермі кремнію під впливом домішок, що легують, точкових дефектів і дислокацій. Встановлено параметри дифузії домішок, умови їх виникнення та видалення в процесі спрямованої кристалізації та в посткристалізаційний період. Показано доцільність легування сонячного кремнію бором та фосфором. З'ясовано механізми ліквідації структурних дефектів. Визначено рухливість та час життя носіїв заряду в досконалих монокристалах кремнію в умовах радіаційного впливу. Показано доцільність застосування кремнію *p*-типу як матеріалу бази сонячних модулів космічного призначення.